Clays and Clay Minerals, Vol. 53, No. 3, 234–249, 2005.

LOSSES OF RADIOGENIC ^{40}Ar IN THE FINE-CLAY SIZE FRACTIONS OF SEDIMENTS

ABRAHAM LERMAN[1] AND NORBERT CLAUER[2]

[1] Department of Geological Sciences, Northwestern University, Evanston, Illinois 60208, USA
[2] Centre de Géochimie de la Surface (CNRS/ULP) 1, rue Blessig, 67084 Strasbourg, France

Abstract—The common observation that smaller particle-size fractions of sedimentary rocks yield younger K-Ar apparent ages than the larger particle-size fractions of the same stratigraphic age was analyzed with the aid of the $^{40}Ar/^{40}K$ ratio from 14 stratigraphically and regionally different sections. Estimation of the loss of radiogenic ^{40}Ar from varied clay-rich size fractions was based on two models: a relationship between particle size and the $^{40}Ar/^{40}K$ ratio, and a theoretical diffusional loss from spherical particles. The differences between the two models and reconciliation of their results are discussed. For the smallest fractions (up to <0.5 μm), percent-wise losses of ^{40}Ar from the spherical particles model increase from Upper Carboniferous and Permian (38±10%), to Late Triassic (47±10%), and to Miocene and Late Neogene (65±8%). This trend suggests that escape of ^{40}Ar from the smaller particles in older sediments decreased or even stopped after deposition of the sedimentary sections.

The large ^{40}Ar losses derived from small $^{40}Ar/^{40}K$ ratios in the younger Tertiary sediments, indicate that addition of K to the small fractions is, at least in part, responsible for the young K-Ar apparent ages in geologically different settings. In several 10^2-10^3 m thick sections, authigenic illite in the <0.1 to <2 μm fractions yields young K-Ar apparent ages resulting from simultaneous ^{40}Ar production and release during clay authigenesis. In a production and loss model, a first-order escape-rate parameter (ε) was estimated at 0.2×10^{-8} to 4×10^{-8} y^{-1}, depending on the K-Ar apparent age of the size fractions and the stratigraphic age of the section. The limitations and uncertainties of the methods of evaluating diagenetic ^{40}Ar losses from fine clay particles are discussed.

Key Words—^{40}Ar Loss, Age, Carboniferous, Clay Fraction, Diffusion, ^{40}K, Miocene, Neogene, Permian, Triassic.

INTRODUCTION

Concentration ratios of radiogenic ^{40}Ar relative to its parent ^{40}K occurring in most Al-Si minerals have been used in various ways in the interpretation of depositional episodes and diagenetic histories of sedimentary sequences. In closed systems where ^{40}Ar forms by radioactive decay of ^{40}K and where neither of the two nuclides escapes or is added, the $^{40}Ar/^{40}K$ ratios allow calculation of meaningful mineral ages. Whereas K-Ar ages in igneous minerals agree well with those obtained by other isotopic methods, K-Ar data from sedimentary mineral fractions often differ from their stratigraphic age because of an occurrence of heterogeneous detrital and diagenetic minerals, involving dissolution of K-rich silicates, precipitation of authigenic K-rich clays, and/or escape of radiogenic ^{40}Ar (Dalrymple and Lanphere, 1969; Faure, 1986). Because of such differences in the stratigraphic age, the K-Ar results in sediment fractions may be referred to either as "dates" as suggested by Faure (1986), or as 'apparent ages'.

Escape of Ar and/or addition of K reduce the $^{40}Ar/^{40}K$ ratio and the computed K-Ar apparent age of mineral fractions or sedimentary aggregates. In continental weathering, K-feldspars and micas are altered to clay minerals with a concomitant loss of radiogenic ^{40}Ar (Clauer *et al.*, 1982). Transformation of smectite to illite in deep sediments is expected to be at the expense of K present in the system (host sediment), probably released from nearby altered coarse-grained minerals; neoformation of illite probably requires addition of K to the system. In any case, transformation (solid-state modification) or neoformation (precipitation) of clay minerals, as well as related alteration and dissolution of K-feldspar and mica, are also expected to induce an escape of radiogenic ^{40}Ar from the solid (*e.g.* Hower *et al.*, 1976).

K-Ar or $^{40}Ar/^{39}Ar$ data of sediment minerals which imply ages that are greater than the stratigraphic age indicate that they already contained radiogenic ^{40}Ar at the time of deposition. Many studies dealing with this aspect are available, involving either the K-Ar (*e.g.* review in Clauer and Chaudhuri, 1995) or the $^{40}Ar/^{39}Ar$ method (Dong *et al.*, 1995, 1997, 2000). The purpose of this paper is not to preferentially select examples from one of these methods, but rather to elaborate on available analytical results from those studies in which the $^{40}Ar/^{40}K$ ratio of detrital clay material can be followed in several size fractions, through burial over hundreds of meters. Alternatively, K-Ar data which give ages for size

* E-mail address of corresponding author:
alerman@northwestern.edu
DOI: 10.1346/CCMN.2005.0530304

fractions which are younger than the stratigraphic age of their host rocks indicate that processes other than a simple loss of radiogenic ^{40}Ar induced the age difference, *e.g.* precipitation of new minerals after deposition, which might have gained K and favored the escape of radiogenic ^{40}Ar from altered framework minerals. In fact, the loss of radiogenic ^{40}Ar from sedimentary minerals includes: (1) diagenetic changes in clastic sediments (Hower *et al.*, 1976; Mitchell and Taka, 1984; Weaver and Broekstra, 1984; Reuter, 1987; Eberl, 1993); and (2) an increased mobility of Ar in crystals when the geothermal gradient increases, at least in the smaller fractions (Langley, 1978; Aronson and Lee, 1986; Liewig *et al.*, 1987; Hamilton *et al.*, 1989; Mossmann *et al.*, 1992; Clauer *et al.*, 1995, 2003; Folger *et al.*, 1995, 1998; Hall *et al.*, 1997).

Again, among the K-Ar and $^{40}Ar/^{39}Ar$ studies, the focus is not on a preferential selection of one particular method, but on those studies most suited to our theoretical analysis. It might be recalled that the $^{40}Ar/^{39}Ar$ method, despite a number of interesting studies, is still not routinely applied to clay-sized material. Even if evaluated by encapsulation, the loss of ^{39}Ar due to recoil might introduce uncertainties in the age calculations, and it has not yet been related to structural changes in the mineral structures. On the other hand, it has yet to be demonstrated that irradiation does not disturb the ^{40}Ar, even if many authors agree on this point. Alternatively, the elaboration of a mathematical model for ^{40}Ar loss in fine clay material, with many controlling factors which are not easy to identify or to evaluate, is a challenging task. Therefore, it appears appropriate to start with a method that provides the best information for the model analysis, even if in this case the K-Ar method may appear as an old, routine method. Of course, calculation of the escaped ^{40}Ar depends directly on the way in which the K-Ar values and the $^{40}Ar/^{40}K$ ratios are determined. Analytical controls in the selected studies ensure that the results used here were well constrained.

Sediments in various settings, ranging from the late Carboniferous to late Neogene, were selected because they report $^{40}Ar/^{40}K$ ratios and K-Ar results over hundreds of meters in samples divided into size fractions from <0.2 μm upwards. The decrease in the $^{40}Ar/^{40}K$ ratios of the small fractions is interpreted as size-related ^{40}Ar loss from progressively altered frame minerals, but addition of K, especially in the smallest fractions possibly enriched in authigenic material, was not excluded. This addition is known to be, at least in part, responsible for the younger K-Ar apparent ages and lower $^{40}Ar/^{40}K$ ratios. Authigenic illite and mixed-layer illite-smectite (I-S) yield K-Ar apparent ages younger than the stratigraphic age in some of these sedimentary sections. To address this aspect, we present a model that analyzes the $^{40}Ar/^{40}K$ ratios as a balance of production and escape of radiogenic ^{40}Ar.

PARTICLE SIZE AND ^{40}Ar CONTENT

Smaller $^{40}Ar/^{40}K$ ratios in the smaller size fractions may give computed ages that are 10^0 to 10^1 Ma younger than in the larger fractions of sedimentary samples (Perry, 1974; Faure, 1986; Schaltegger *et al.*, 1995; Huon *et al.*, 1993; Clauer *et al.*, 1999; also Tables 1, 2). Although it is possible that some of the smaller particles are newly formed, the mineralogy and morphology of the size fractions do not always clearly indicate whether the small particles are younger or of the same age as the large ones. Our view is that lower $^{40}Ar/^{40}K$ ratios in the smaller fractions result from ^{40}Ar loss, probably due to a shorter diffusion path than in the larger particles. Computation of such losses by a number of investigators was aimed at establishing timescales of heating events due to burial, igneous intrusions, tectonic stresses, or hot-fluid migrations that caused accelerated losses of ^{40}Ar, thereby resetting the K-Ar clock (*e.g.* Turner, 1968; Dodson, 1973; Lovera, 1992). In this section, we address the issue of $^{40}Ar/^{40}K$ ratios and K-Ar apparent ages of varied size fractions that, according to the literature, have not been heated above 175°C since deposition. As detailed in a later section, the diffusional flux across particle boundaries depends on the surface area, and the mass loss depends on the surface area to volume ratio, both being functions of the particle shape and size.

The studied sequences are of Upper Carboniferous (Schaltegger *et al.*, 1995), Permian (Zwingmann *et al.*, 1999), Upper Triassic (Huon *et al.*, 1993), Miocene (Perry, 1974), and Upper Neogene (Furlan *et al.*, 1996) stratigraphic ages. The K-Ar dates are reported on the basis of the K content, the calculated ^{40}K amount and the concentration of radiogenic ^{40}Ar corrected for any atmospheric contamination (Tables 1, 2). The uncertainty of the K-Ar values is 2−3% of the reported value. For the eight stratigraphically different samples (Table 1), the reported K-Ar dates were recalculated to the $^{40}Ar/^{40}K$ ratios (Table 2). From Table 2, the K-Ar apparent age is older than the stratigraphic age for the samples from late Neogene of Kalimantan, Miocene of the Gulf Coast, and late Triassic of Morocco, whereas the Permian of Germany and the Upper Carboniferous of Switzerland yield K-Ar data younger than the stratigraphic age. Although these relationships between the K-Ar apparent and stratigraphic age suggest different types for the fine and coarse fractions of the different formations, we address the Ar loss in the finest fraction relative to the larger. Different size fractions may contain different proportions of K minerals, *e.g.* more illite in the clay fraction and more K-feldspar in the coarser fractions. Therefore, the different K concentrations result in different concentrations of ^{40}Ar produced over time, and the ^{40}Ar content in the different size fractions must be normalized to the K content. The $^{40}Ar/^{40}K$ ratio gives ^{40}Ar concentration per unit of ^{40}K

Table 1. ^{40}Ar loss from the smallest size fraction relative to the larger size fraction as shown in Column C. R is the $^{40}Ar/^{40}K$ ratio in Table 2 for the size fractions used, a is particle radius (μm). Loss in Column E is computed from equation 3. Detailed data are given in Table 2.

A Stratigraphic age and reference	B Unit name, depth, other designation	C Particle-size range (diameter, μm)	D Linear fit $\ln R = A + b \ln a$	E ^{40}Ar loss from apparent age (%)
Neogene, Mahakam, Borneo, Furlan (1994)	Misedor 183 m (Mahakam 1)	<0.2 to 20–40	$A = -5.209$ $b = 0.080$	41
Miocene, Gulf Coast, USA Perry (1974)	4417 m (Gulf Coast 3)	from <0.5 to 2–10	$A = -4.340$ $b = 0.220$	50
	5523 m (Gulf Coast 4)	from <0.5 to 2–10	$A = -4.704$ $b = 0.213$	49
Upper Triassic, Morocco Huon *et al.* (1993)	Sample T1 (Triassic 1 Morocco)	from <0.4 to 10–20	$A = -4.134$ $b = 0.081$	39
	Sample T2 (Triassic 2 Morocco)	from <0.4 to 10–20	$A = -4.086$ $b = 0.058$	33
Permian (Rotliegende) North Germany Zwingmann (1995), Zwingmann *et al.* (1999)	4594.3 m Sample 4 (Permian 1 Germany)	from <0.2 to 10–20	$A = -4.459$ $b = 0.029$	15
	4657.7 m Sample 6 (Permian 2 Germany)	from <0.2 to 10–20	$A = -4.423$ $b = 0.043$	22
U. Carboniferous (Stephanian), North Switzerland Schaltegger *et al.* (1995)	Sample 3544 1775 m (U. Carb. 1 Switzerland)	from <0.2 to 2–6	$A = -4.381$ $b = 0.093$	26

mass in the particle; it is not affected by the differences in the K contents of the fractions where ^{40}Ar loss began at the same time. As radiogenic ^{40}Ar and K amounts in minerals are measured to determine the $^{40}Ar/^{40}K$ ratios, the K-Ar data of the varied fractions in a sequence provide the necessary information on the $^{40}Ar/^{40}K$ ratios and normalized ^{40}Ar contents.

The $^{40}Ar/^{40}K$ ratio of each fraction is shown as a function of the particle radius in three late Paleozoic, two Mesozoic, and three Tertiary samples (Tables 1, 2; Figure 1). The linear regressions of data from different stratigraphic ages and locations are also given in the form of:

$$\ln R = A + b \ln a \quad (1)$$

where R is the $^{40}Ar/^{40}K$ ratio, a is the mean particle radius in μm, b is the slope of the regression line, and A is a constant for each line. The plots show that the larger fractions have greater $^{40}Ar/^{40}K$ ratios with the magnitude of the change from smallest to biggest size given by the steepness of the slope or the coefficient b in equation 1. The $^{40}Ar/^{40}K$ ratios in two fractions of any sediment, of mean radii a_1 and a_2, are related by equation 1 as:

$$\ln R_1/R_2 = b \ln a_1/a_2 \quad (2)$$

where subscript 1 denotes the smallest and subscript 2 a larger fraction. The fraction of ^{40}Ar that escaped from the smaller size fraction relative to the larger one is approximated by using equation 2:

$$f = 1 - R_1/R_2 = 1 - (a_1/a_2)^b \quad (3)$$

For the data in Table 1, the mean radius of the smallest fraction varies from 0.05 (<0.2 μm fraction) to 0.125 μm (<0.5 μm fraction). The larger fractions vary even more from one section to another: in the Upper Carboniferous the largest fraction is 2–6 μm giving a mean radius $a = 2$ μm, in the Neogene of the Gulf Coast, the largest size fraction is 2–10 μm giving a mean radius of $a = 3$ μm. Because of these differences, the larger size fractions were taken at 10–20 to 20–40 μm to make the range of sizes close to the narrow size distributions. Calculation of the amount of ^{40}Ar lost

Table 2. Data in columns B–D are from the references listed in column A. Data in columns E and F computed from column D, equation 10. Data in columns G and H are from column C. Column I: values of the linear regression slopes, equation 8 and Figure 2, from the data in columns F and H. Column J: linear correlation coefficient for the data in columns F and H for all the particle sizes in the sample (correlation limit = −1). Column K: computed fractions of ^{40}Ar escaped from different particle-size classes, equation 9 and Figure 3. Ages of stratigraphic units from Harland *et al.* (1990).

A Stratigraphic age and reference	B Unit name, depth, other designation	C Particle-size range (diameter, μm)	D K-Ar apparent age (10^6 y)	E Atomic ratio $R = {}^{40}Ar/{}^{40}K$	F ln R	G Particle mean radius a (μm)	H $1/a^2$ (μm^{-2})	I Slope of ln R *vs.* $1/a^2$ $-D\pi^2 t$ (μm^2)	J Linear correlation coefficient	K Fraction of ^{40}Ar escaped (f_r)
Neogene,	Misedor	<0.2	70.4	0.00417	−5.480	0.05	400	−0.0007	−0.766	56.1%
Mahakam, Borneo	183 m	0.2–0.6	88.6	0.00528	−5.245	0.2	25			16.3%
Furlan (1994)	(Mahakam 1)	2–6	93.8	0.00559	−5.186	2	0.25			2.4%
Age marker: 18 My		6–10	98.6	0.00589	−5.135	4	0.0625			
(at 4000 m)		10–20	96.7	0.00577	−5.155	7.5	0.0178			
		20–40	117.6	0.00706	−4.953	15	0.0044			
		40–63	126.5	0.00761	−4.878	25.75	0.0015			
	HQ2	<0.2	57.4	0.00339	−5.687	0.05	400.0	−0.0014	−0.810	73.0%
	1003.75 m	0.2–0.6	89.6	0.00534	−5.233	0.2	25.0			23.0%
	(Mahakam 2)	2–6	104.9	0.00628	−5.071	2	0.25			2.6%
		6–10	151.4	0.00918	−4.691	4	0.0625			
		10–20	176.1	0.01075	−4.533	7.5	0.0178			
		20–40	137.0	0.00827	−4.795	15	0.0044			
		40–63	112.1	0.00672	−5.003	25.75	0.0015			
Miocene	1582 m	<0.5	164	0.00997	−4.608	0.125	64	−0.0122	−0.991	71.5%
Gulf Coast, USA	(Gulf Coast 1)	0.5–2	312	0.01979	−3.923	0.625	2.56			18.1%
Perry (1974)		2–10	358	0.02301	−3.772	3	0.11			4.2%
Age marker:										
5.2(?)–23.3 My	2331 m	<0.5	165	0.01004	−4.601	0.125	64	−0.01104	−0.990	69.1%
	(Gulf Coast 2)	0.5–2	295	0.01862	−3.983	0.625	2.56			17.3%
		2–10	336	0.02146	−3.842	3	0.11			4.1%
	4417 m	<0.5	137	0.00827	−4.795	0.125	64	−0.0085	−0.881	63.0%
	(Gulf Coast 3)	0.5–2	191	0.01171	−4.448	0.625	2.56			15.3%
		2–10	266	0.01665	−4.095	3	0.11			3.3%
	5523 m	<0.5	100	0.00597	−5.120	0.125	64	−0.0077	−0.814	60.6%
	(Gulf Coast 4)	0.5–2	129	0.00777	−4.858	0.625	2.56			14.5%
		2–10	192	0.01177	−4.442	3	0.11			3.2%

Upper Triassic	Sample T1	<0.4	195	0.01196	−4.426	0.1	100	−0.0032	−0.843	57.4%
Morocco	(Triassic 1	0.4−1	244	0.01518	−4.188	0.35	8.16			19.0%
Huon *et al.* (1993)	Morocco)	1−2	260	0.01625	−4.120	0.75	1.78			9.2%
Age marker:		2−5	275	0.01726	−4.059	1.75	0.3265			4.1%
200−220 My		5−10	299	0.01889	−3.969	3.75	0.0711			
		10−20	308	0.01951	−3.937	7.5	0.0178			
		20−300	329	0.02097	−3.865	80	0.0002			
	Sample T2	<0.4	224	0.01386	−4.279	0.1	100	−0.0016	−0.631	48.2%
	(Triassic 2	0.4−1	293	0.01848	−3.991	0.35	8.16			15.5%
	Morocco)	1−2	232	0.01438	−4.242	0.75	1.78			7.4%
		2−5	264	0.01652	−4.103	1.75	0.3265			3.3%
		5−10	305	0.01931	−3.947	3.75	0.0711			
		10−20	323	0.02055	−3.885	7.5	0.0178			
		20−300	322	0.02048	−3.888	80	0.0002			
Upper Triassic	Sample 3537	<0.2	146	0.00884	−4.729	0.05	400	−0.00074	−0.695	49.6%
(Keuper)	(Triassic 1	0.2−0.4	163	0.00991	−4.614	0.15	44.4			18.6%
North Switzerland	Switzerland)	0.4−2	231	0.01432	−4.246	0.6	2.78			4.9%
Schaltegger *et al.*		2−6	177	0.01081	−4.528	2	0.25			1.7%
(1995)										
Age marker:										
208−237 My										
	Sample 3539	<0.2	177	0.01081	−4.528	0.05	400	−0.00034	−0.849	35.5%
	(Triassic 2	0.2−0.4	188	0.01151	−4.464	0.15	44.4			12.7%
	Switzerland)	0.4−0.8	196	0.01203	−4.420	0.3	11.1			6.6%
		0.8−2	203	0.01248	−4.383	0.7	2.04			3.1%
		2−6	209	0.01287	−4.353	2	0.25			1.5%
Permian (Rotliegende),	4594.3 m	<0.2	178.2	0.01088	−4.521	0.05	400	−0.00007	−0.439	29.6%
Northern Germany	Sample 4	0.2−0.6	185.7	0.01136	−4.477	0.2	25			7.9%
Zwingmann (1995),	(Permian 1	0.6−1	180.2	0.01101	−4.509	0.4	6.25			4.1%
Zwingmann *et al.*	Germany)	1−2	181.2	0.01107	−4.503	0.75	1.78			2.3%
(1999)		2−6	185.6	0.01136	−4.478	2	0.25			1.1%
Age marker:		6−10	195.7	0.01201	−4.422	4	0.0625			
260−290 My		10−20	207.8	0.01280	−4.359	7.5	0.0178			
		20−40	199.5	0.01226	−4.402	15	0.0044			
		40−63	212.0	0.01307	−4.337	25.75	0.0015			
		>63	210.4	0.01297	−4.345					

Table 2 (*contd.*)

A Stratigraphic age and reference	B Unit name, depth, other designation	C Particle-size range (diameter, μm)	D K-Ar apparent age (10^6 y)	E Atomic ratio $R = {}^{40}Ar/{}^{40}K$	F ln R	G Particle mean radius a (μm)	H $1/a^2$ (μm^{-2})	I Slope of ln R *vs.* $1/a^2$ $-D\pi^2 t$ (μm^2)	J Linear correlation coefficient	K Fraction of ^{40}Ar escaped (f_r)
	4657.7 m	<0.2	166.1	0.01011	−4.594	0.05	400	−0.00043	−0.803	44.3%
	Sample 6	0.2–0.6	186.7	0.01143	−4.472	0.2	25			12.4%
	(Permian 2	0.6–1	193.6	0.01187	−4.433	0.4	6.25			6.3%
	Germany)	1–2	193.2	0.01185	−4.436	0.75	1.78			3.4%
		2–6	203.5	0.01252	−4.381	2	0.25			1.6%
		6–10	211.6	0.01304	−4.339	4	0.0625			
		10–20	210.3	0.01296	−4.346	7.5	0.0178			
		20–40	212.9	0.01313	−4.333	15	0.0044			
		40–63	221.3	0.01368	−4.292	25.75	0.0015			
		>63	219.3	0.01355	−4.302					
U. Carboniferous	Sample 3544	<0.2	152	0.00921	−4.687	0.05	400	−0.00069	−0.816	48.2%
(Stephanian),	1775 m	0.2–0.4	166	0.01010	−4.595	0.15	44.4			18.0%
North Switzerland	(U. Carb. 1	0.4–0.8	193	0.01184	−4.437	0.3	11.1			9.2%
Schaltegger *et al.*	Switzerland)	0.8–2	212	0.01307	−4.337	0.7	2.04			4.0%
(1995)		2–6	202	0.01242	−4.389	2	0.25			1.5%
Age marker: 299–306 My										
	Sample 3545	<0.2	168	0.01023	−4.582	0.05	400	−0.00021	−0.886	28.6%
	1962 m	0.2–0.4	177	0.01081	−4.528	0.15	44.4			10.1%
	(U. Carb. 2	0.4–0.8	180	0.01100	−4.510	0.3	11.1			5.1%
	Switzerland)	0.8–2	187	0.01145	−4.470	0.7	2.04			2.3%
		2–6	180	0.01100	−4.510	2	0.25			1.1%

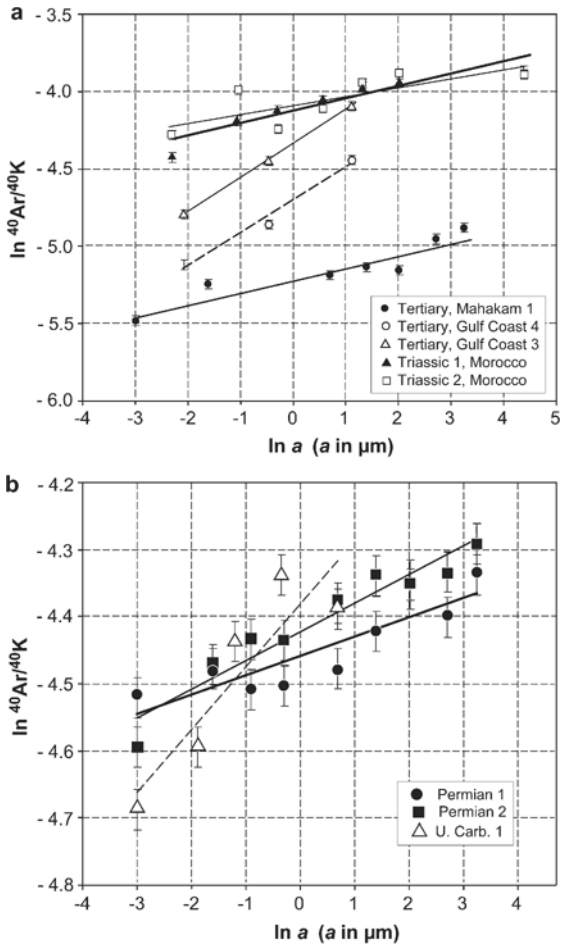

Figure 1. Plot of ln ^{40}Ar/^{40}K ratio *vs.* mean particle size, ln *a* (particle radius, *a*, in μm) for sediments of different ages and geological settings. The data are from Table 2 and the slopes of linear regression lines are from Table 1. Error bars are ±3% of the ^{40}Ar/^{40}K ratio or ±0.03 of its ln value. Note the difference in the vertical scales of parts a and b.

from equation 3 is based on the ratios R_1 and R_2 for each fraction. The values of the fractional losses calculated from equation 3 depend on the available data for the large particle size, a_2. For a_2 values near or above the upper end of the size range, the linear regression equation increases the fraction of lost ^{40}Ar, *f*.

The differences between the samples of varied ages and locations result from the scatter of the data points, the varied size intervals used by the investigators, and the differences in the slopes of the linear regressions (Figure 1). As a whole, the smallest fractions of the Upper Carboniferous and Permian samples are characterized by the smallest loss (15–26%) relative to the larger 10–20 μm size fractions. The <0.4 μm size fraction of the Upper Triassic sequence shows a somewhat greater loss (33–39%), followed by the Miocene sequence of the Gulf Coast where the estimated loss is ~50% for fractions in a narrow range from <0.5 to 2–10 μm. The results of the ^{40}Ar losses in the finest fractions of each sample (Table 1) should be interpreted relative to variably larger fractions. A different estimate of the losses is discussed in the next section.

^{40}Ar RELEASE FROM SPHERICAL PARTICLES

A simplified model

Different models of Ar loss by diffusion from minerals and size fractions of varied shapes are already available (Turner, 1968; Dodson, 1973; Huon *et al.*, 1993; Clauer *et al.*, 2003). Different shapes, such as spheres, plane sheets and infinite circular cylinders were used in the models. Models of slabs or plane sheets are mathematically much more convenient and easier to use than models of cubes or parallelepipeds, and the same may be said for models of infinitely long cylinders as opposed to cylinders of finite length and volume. In a sphere, diffusion occurs across the whole surface, whereas it is across the two parallel surfaces in a plane sheet and across the cylindrical surface in an infinite circular cylinder. For particles that are big flakes or long cylinders, such models might be reasonable approximations. However, for particles which are nearly equidimensional (shapes approximating a cube or a cylinder of height equal to base diameter), a plane sheet or an infinitely long cylinder may introduce considerable distortion. A model of a plane sheet applied to cube-shaped millimeter-sized mica flakes allows only 1/3 of the particle surface for diffusion across it. In a cylinder of height equal to width, the model allows only 2/3 of total surface for transport across it. It should be borne in mind that the smaller the particles (in the micrometer scale), the better a spherical shape may explain the relative Ar loss.

In the study of ^{40}Ar diffusion from minerals, as developed by Dodson (1973) and used by others, the following conditions apply: an initially uniform and constant ^{40}Ar concentration in the solid (at $t = 0$), and a zero concentration at the particle surface at time $t > 0$. This boundary condition means that ^{40}Ar leaving the particle migrates into a space where its concentration is negligibly low at all times relative to its concentration in the particle. For a spherical particle of radius *a*, fractional loss f_r becomes (Carslaw and Jaeger, 1959, pp. 234–235, IV, (8); Crank, 1967; Dodson, 1973):

$$f_r = 1 - 6\sum_{n=1}^{\infty} \frac{\exp(-n^2\pi^2 Dt/a^2)}{n^2\pi^2} \qquad (4)$$

The fraction of ^{40}Ar escaping from a spherical particle depends on its size (radius *a*), the diffusion coefficient of ^{40}Ar in the particle (*D*, considered constant in the spherical particle), and the duration of the escape process (time *t*). Continuous production of radiogenic ^{40}Ar is not considered here or in models for other particle shapes. The fraction escaped, f_r, is particle-shape dependent: for the sphere and cube, the

difference in the computed fraction at a given value of the dimensionless group parameter Dt/a^2 is ~3% or less; it is 15% or less at the same value of Dt/a^2, for an infinite circular cylinder. However, the computed fraction lost may be up to 40% smaller in a slab or plane sheet than in a sphere (McDougall and Harrison, 1999). Contrary to laboratory experiments of diffusional loss for which initial concentration of ^{40}Ar in the particles, particle size and duration are known, application of equation 4 to heterogeneous aggregates of sediment particles of different stratigraphic ages and with geological histories which are not always well known cannot provide more than a rough estimate of ^{40}Ar lost from size fractions. We make such estimates for the 14 sequences of varied stratigraphic ages (Table 2).

For spherical particles, the fraction of ^{40}Ar remaining in the particles is from equation 4:

$$1-f_r = \frac{6}{\pi^2}\sum_{n=1}^{\infty} e^{-n^2\pi^2 Dt/a^2}/n^2 \approx 0.61\sum_{n=1}^{\infty} e^{-n^2\pi^2 Dt/a^2}/n^2 \quad (5)$$

As an approximation, considering only the first exponential term in equation 5, gives a simpler form of the equation:

$$\ln(1-f_r) \approx \ln\frac{6}{\pi^2} - \frac{D\pi^2 t}{a^2} \quad (6)$$

This approximation is valid for sufficiently large values of the parameter $\pi^2 Dt/a^2$ in equation 5. In general, the molecular diffusion coefficients of Ar and other noble gases in sheet silicates, especially in clays, are only poorly known at temperatures below 250°C. Also not well known is the duration of ^{40}Ar loss from sediment particles that may be either close to the depositional age or much younger. The parameter $\pi^2 Dt/a^2$ is sufficiently large for values of $D \geqslant 5\times10^{-24}$ cm^2 s^{-1}, $t \geqslant 10^7$ y, and particle size $a \leqslant 1$ μm. Ar diffusion coefficients in silicates reported in the literature vary by several orders of magnitude (data compiled by Moffatt, 1969, cited by McDougall and Harrison, 1999; Lerman, 1979; Freer, 1981; Wijbrans and McDougall, 1986), and extrapolation of high-temperature results to lower ones is rather uncertain (Freer, 1981).

The uncertainties in the mineral composition and origin of the size fractions discussed in the preceding section also apply to the sediments discussed here. Using the notation for the normalized ^{40}Ar concentration or the ^{40}Ar/^{40}K ratio, denoted $R = {}^{40}\text{Ar}/{}^{40}\text{K}$ in equation 1, the fraction of ^{40}Ar remaining in a particle is:

$$1-f_r = \frac{R}{R_0} \quad (7)$$

here R_0 is the unknown initial concentration. Using equation 7 in equation 6, the latter becomes:

$$\ln R = \ln\frac{6R_0}{\pi^2} - \frac{D\pi^2 t}{a^2} \quad (8)$$

The preceding relationship can be plotted as ln R, the logarithm of the ^{40}Ar/^{40}K ratio, *vs.* $1/a^2$, the reciprocal of the squared particle radius. The plot is a straight line with a slope equal to $-D\pi^2 t$.

Evaluation of ^{40}Ar data for small particles

Figure 2 shows from equation 8 a number of sample plots of ln R *vs.* $1/a^2$ for the small fractions of $a \leqslant 2$ μm and, correspondingly, $1/a^2$ in the range $0.25 \leqslant 1/a^2 \leqslant 400$. The straight line for each sample represented by three or more data points is the linear best fit to the data plotted in equation 8. Figure 2 addresses only the smaller fractions of $a \leqslant 2$ μm as the larger fractions are relatively very scattered, because they may consist of aggregates of smaller ones and because they are more likely to contain detrital K-feldspar and mica of older ages. The vertical error bars represent ±3% of the K-Ar apparent ages or of the ratio $R = {}^{40}\text{Ar}/{}^{40}\text{K}$, corresponding to ±0.03 of ln R. The linear correlation coefficient for each plot is given in Table 2. A steep slope of the ^{40}Ar/^{40}K ratio *vs.* particle size suggests a stronger decrease in ^{40}Ar with decreasing particle size. A flatter slope suggests a weaker relationship between ^{40}Ar loss and size.

From the slopes of the ln R *vs.* $1/a^2$ plots (Table 2, column I, and Figure 2), it is possible to compute the ^{40}Ar fraction escaped by use of equations 6 and 8:

$$f_r = 1-\frac{6}{\pi^2}\sum_{n=1} e^{-n^2 D\pi^2 t/a^2}/n^2 \approx 1-0.61\sum_{n=1}\frac{\exp(-n^2\times\text{Slope}/a^2)}{n^2} \quad (9)$$

The computed values of f_r (Table 2) for all the sediment suites, are shown for a number of representative samples with sizes mostly $a \leqslant 2$ μm (Figure 3). The older Upper Carboniferous and Permian sediments show smaller ^{40}Ar losses from fine fractions with a mean of ~38% (range 29–48%), than the younger late Triassic sediments of Morocco and Switzerland in which the loss averages 48% (range 36–57%). The smaller fractional losses in the older sediments may reflect a stop of the ^{40}Ar escape at some time allowing for some buildup since then. Although a loss of 40–65% of ^{40}Ar corresponds to the initial ^{40}Ar/^{40}K ratios being greater than the measured values (Table 2, column E) by a factor of 1.7 to 2.9, it does not necessarily mean that the true ages of the smallest particles are greater by the same factor than their K-Ar apparent ages (Table 2, column D). The major reason for not assigning a correspondingly greater age to the smallest fractions is

that the lost ^{40}Ar in the range 60–73% in the late Neogene of Kalimantan and in the Miocene of the Gulf Coast confirms that K was not only conserved in the fine fractions, but added to it after deposition, thereby reducing the $^{40}Ar/^{40}K$ ratio and the K-Ar apparent age. In fact, apparent high fractional losses of ^{40}Ar computed from the model appear to be an indirect indication of K addition during diagenesis.

APPARENT AGE IN RELATION TO STRATIGRAPHIC AGE

Newly formed K-rich clays were identified in all smaller fractions of the Permian, Mesozoic and Tertiary sediments (Table 3). Besides morphological evidence, these small fractions have K-Ar apparent ages which are younger than the stratigraphic age of the sections, and their $^{40}Ar/^{40}K$ ratios show little or no trend, varying about a mean value in up to 1500 m thick units. In the case of the North Sea section with clay K-Ar apparent ages younger than the stratigraphic age (Figure 4), the K-Ar values of the smaller fractions probably indicate mineral neoformation with some escape of radiogenic ^{40}Ar. The duration of the ^{40}Ar production and escape lasted over a period of time that should not be greater than the stratigraphic age and not less than the K-Ar apparent age. The scatter of the K-Ar data (Table 3 and Figure 4) is attributable to varying proportions of illite and I-S in the fine fractions, the occurrence of partly altered K silicates in the coarser fractions, and the occurrence of detrital mica with K-Ar apparent ages from much older Paleozoic sources (Glasmann *et al.*, 1989). In fact, the range of the $^{40}Ar/^{40}K$ ratios is generally greater than the change expected in a closed system over a period of 10^7 to 10^8 y: an increase in the $^{40}Ar/^{40}K$ ratio with no radiogenic ^{40}Ar present initially would be 6×10^{-4} to 6×10^{-3}, which is smaller than the range of $\pm 10^{-1}$ in the data (Table 3).

The Permian sandstones of northern Germany taken between 4595 and 4855 m contain authigenic illite

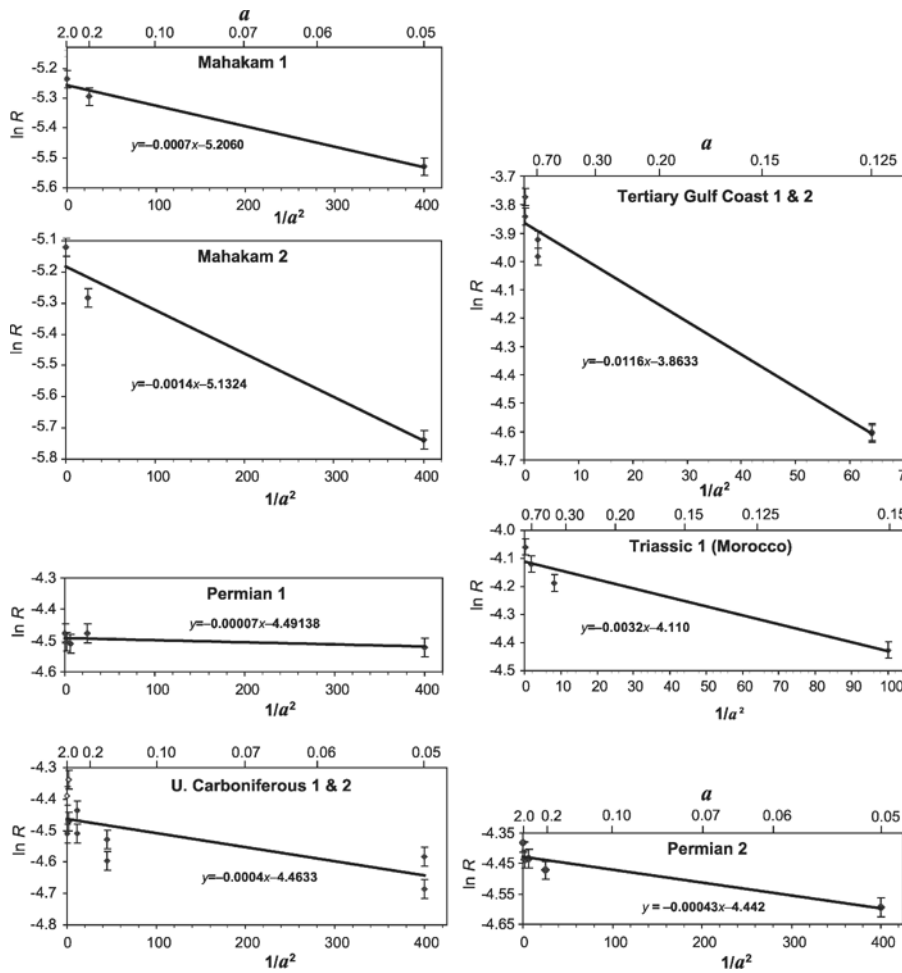

Figure 2. Plots of the logarithm of the $^{40}Ar/^{40}K$ ratio (ln R) *vs.* particle size ($1/a^2$) for sizes $a \leqslant 2$ μm. In the best-fit equations: y is ln R, x is $1/a^2$. Solid lines and equations are best fit to the particle sizes shown (particle radius $a \leqslant 2$ μm). Data in Table 2, equation 8.

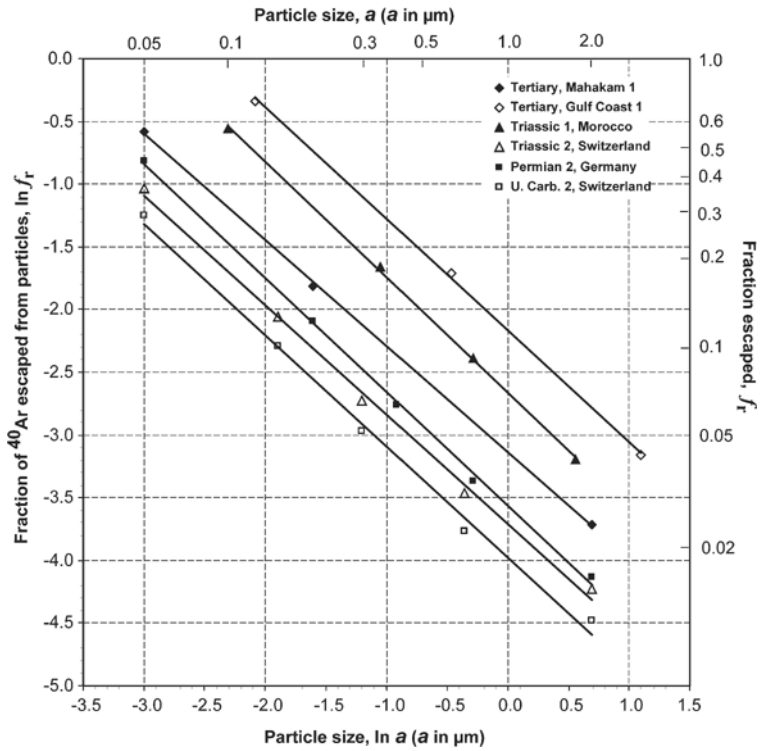

Figure 3. Fractional loss of ^{40}Ar as a function of particle size for sediments of different ages and geological settings. Data in Table 2, column K, and equation 9.

which is filling secondary porosity with *in situ* temperatures of 150ºC at 5000 m (Liewig and Clauer, 2000). These illite infillings occur as coatings on authigenic quartz and as radial growths in the pore space of the rocks. For a stratigraphic age interval of 260–290 Ma, the 184–204 Ma K-Ar ages of <2 μm illite reflect either one continuous or two distinct episodes of nucleation and growth. The Huldra field in the North Sea (Table 3, Figure 4) extends from 2500 to 4200 m in Mesozoic sediments (from 80 to >160 Ma) at a temperature range of 90–160ºC. The <0.1 μm fraction consists of >90% of I-S mixed with illite, chlorite and kaolinite, and it yields K-Ar apparent ages of ~78 Ma. Glasmann *et al.* (1989) also estimated a detrital contribution from older particles to this <0.1 μm fraction and arrived at a somewhat younger 'corrected illite age' of 55–70 Ma. In the well known study of clay diagenesis in the Gulf Coast sediments, Aronson and Hower (1976) described authigenic I-S between 3700 and 5500 m at temperatures of 95–175ºC. The Miocene-Oligocene boundary of the section is at 2200 m, between 25 and 22.9 Ma (Aronson and Hower, 1976; Harland *et al.*, 1990; Shackleton *et al.*, 2000; Wilson *et al.*, 2002). The approximate stratigraphic age of the deeper

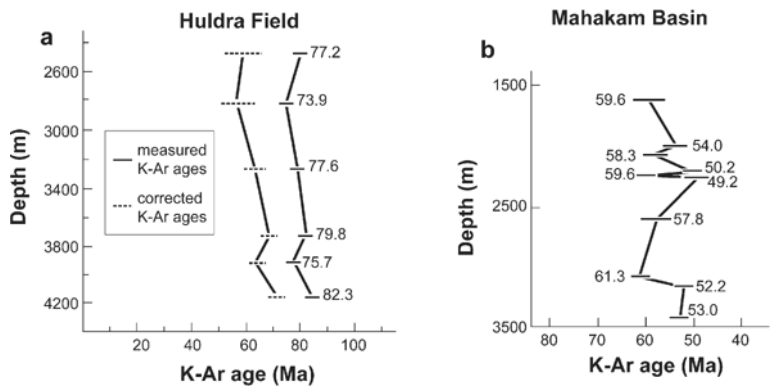

Figure 4. (a) Plot of K-Ar apparent ages, younger than the stratigraphic age, as a function of sediment depth at Huldra Field, Bergen High Area, North Sea (Table 3; from Glasmann *et al.*, 1989). (b) Plot of K-Ar apparent ages, older than the stratigraphic age, in the <0.4 μm fraction of the shales in the Mahakam Delta Basin, Borneo (Table 3, from Clauer *et al.*, 1999).

Table 3. $^{40}Ar/^{40}K$ ages in sediment sections that are nearly constant with depth, the range of variation shown as the plus or minus age. The $^{40}Ar/^{40}K$ atomic ratios are computed from the radiogenic ages cited using equation 10. Next to the value of ε the assumed starting time of the process is shown in parenthesis.

Location	Sediment depth (m)	Stratigraphic age (10^6 y)	$^{40}Ar/^{40}K$ age (10^6 y)	$^{40}Ar/^{40}K$ ratio ($\times 10^{-3}$)	Mineralogy and comments	Reference	^{40}Ar escape-rate parameter ε (10^{-8} y^{-1})
Soehlingen, N. Germany	4595–4645	Permian (Rotliegendes, 260–290 My)	184±7	11.2 ± 0.4	Fraction 0–2 μm, illite, samples 1, 2a	Liewig and Clauer (2000)	0.33 (275 My)
	4645–4855	same	204±6	12.6 ± 0.4	Fraction 0–2 μm, illite, samples 2b, 3a	same	0.23 (275 My)
North Sea, Bergen High area Huldra Field	2550–4200	Cretaceous and older (80–>160 My)	78±4	4.62 ± 0.23	Shale illite, <0.1 μm size fraction	Glasmann *et al.* (1989)	0.53 (100 My) 0.80 (120 My) 1.06 (160 My)
same	same	same	55 to 70	——	'Corrected illite age'	same	——
Gulf Coast, USA	3700–5500	Upper Oligocene (30–34 My; Miocene–Oligocene boundary at 2200 m, 23–25 My)	18.4±2	1.08 ± 0.1	Illite-smectite, <0.1 μm size fraction	Aronson and Hower (1976)	2.6 (25 My) 3.8 (32 My)
Mahakam Delta Basin, Handil Field, Eastern Borneo	180–2000	Pleistocene (?) to Middle Miocene) (18 My at 4000 m	95±5	5.7 ± 0.3	Shales, 2–20 μm size fraction	Furlan (1994), Furlan *et al.* (1996)	——
same (wells HD1, HR1, HRbis KB1)	1600–2500	same	55±6	3.2 ± 0.3	Shales, <0.4 μm size fraction	Clauer *et al.* (1999)	——

3700–5500 m section is 30 to 34 Ma. The minerals of the <0.1 μm fraction have a mean K-Ar apparent age of 18 Ma (Table 3). It was shown to contain added K, although the authors stated that "it is also possible that some degassing of radiogenic argon has occurred from the finest fraction of the deepest shale".

As contrasted with the three sections that show the small-size authigenic fraction younger than the stratigraphic age, the shale unit at 4000 m depth in the late Neogene of Kalimantan provides K-Ar apparent ages greater than the stratigraphic age with values of ~55 Ma in the <0.4 μm fraction (Figure 4) and values of ~95 Ma in the 2–20 μm fraction. The <0.4 μm fraction consists of variable proportions of I-S, illite, chlorite and kaolinite, whereas the coarse fraction comprises quartz, micas and minute amounts of plagioclase and K-feldspar. The sequence is characterized by sedimentation of material that originated in the mountains built around the basin 90–100 Ma ago (Furlan *et al.*, 1996). A reference stratigraphic marker of ~18 Ma was identified at a depth of ~4000 m (Priyomarsono, 1985). The temperature is 60–80ºC between 1100 and 2000 m. The coarser 2–20 μm fraction has a $^{40}Ar/^{40}K$ ratio close to that of the source terrain (Table 3). The heterogeneous nature of the <0.4 μm fraction is further confirmed by identification using scanning electron microscopy of authigenic platelets on larger detrital particles (Clauer *et al.*, 1999). A study of fundamental particles separated from I-S of sandstones buried at 4000 m estimated the K-Ar apparent age of the authigenic platelets at ~14 Ma, again younger than the stratigraphic age (Clauer *et al.*, 2004). In the next section we address the younger K-Ar apparent ages of the authigenic small fractions as a combination of production and escape of radiogenic ^{40}Ar.

PRODUCTION AND ESCAPE OF ^{40}Ar

Closed system

In a closed system that initially contains no radiogenic ^{40}Ar, decay of ^{40}K to ^{40}Ar results in the $^{40}Ar/^{40}K$ atomic or mass ratio increasing with time according to

the following relationship (*e.g.* Faure, 1986):

$$\frac{^{40}\mathrm{Ar}}{^{40}\mathrm{K}} = \frac{\lambda_a}{\lambda}(e^{\lambda t} - 1) \tag{10}$$

where $\lambda_a = 0.581 \times 10^{-10}$ y^{-1} is the decay rate constant of ^{40}K to ^{40}Ar (*e.g.* Steiger and Jäger, 1977), and t is the time that starts with ^{40}K decay and ^{40}Ar accumulation in the closed system. Time t can be computed from the measured ^{40}Ar/^{40}K ratio. If the system initially contains ^{40}Ar, then equation 10 becomes:

$$\begin{aligned}\frac{^{40}\mathrm{Ar}}{^{40}\mathrm{K}} &= \left(\frac{\lambda_a}{\lambda} + \frac{^{40}\mathrm{Ar}_0}{^{40}\mathrm{K}_0}\right)e^{\lambda t} - \frac{\lambda_a}{\lambda} \\ &= \left(0.1048 + \frac{^{40}\mathrm{Ar}_0}{^{40}\mathrm{K}_0}\right)e^{\lambda t} - 0.1048\end{aligned} \tag{11}$$

where subscript 0 denotes the initial concentrations of ^{40}Ar and ^{40}K in the particles. Initial $(^{40}\mathrm{Ar}/^{40}\mathrm{K})_0$ ratios that develop prior to deposition in particles of ages 10^7 to 10^8 y, as closed systems, are of orders of magnitude 0.001 to 0.01. Although these are smaller than the term $\lambda_a/\lambda = 0.105$, they are often ignored because they are not always known. The ^{40}Ar/^{40}K ratio increases with an increasing age, where a change of a few percent in the ratio corresponds to a similar percent-wise change in the computed age.

Open system

In an open system, ^{40}Ar is produced by decay of ^{40}K and its loss may be considered as a fractional rate ε (y^{-1}), where the balance between production, Q, and loss is:

$$\frac{d(^{40}\mathrm{Ar})}{dt} = Q - \varepsilon\ ^{40}\mathrm{Ar} \tag{12}$$

where the production rate of radiogenic ^{40}Ar, Q, is equal to an exponentially decreasing decay rate of ^{40}K to ^{40}Ar:

$$Q = \lambda_a\ ^{40}\mathrm{K}_0 e^{-\lambda t} \tag{13}$$

The units of production and loss rates are, for example, in mol ^{40}Ar g^{-1} of sediment per unit of time. $^{40}\mathrm{K}_0$ is the initial concentration. From the production rate term given in equation 13, the relative rate of change in the production rate is:

$$\frac{d\ln Q}{dt} = -\lambda = -5.543 \times 10^{-10}\ \mathrm{y}^{-1} \tag{14}$$

At a timescale of 10^7 y, the ^{40}Ar production rate decreases by ~0.5% and the ^{40}K concentration decreases by the same amount. Because the decrease in the production rate is small at such time scales, it may be considered approximately constant. Substitution of equation 13 in equation 12 and integration of equation 12 gives the ^{40}Ar/^{40}K ratio that changes with time according to the following relationship:

$$\frac{^{40}\mathrm{Ar}}{^{40}\mathrm{K}} = \frac{\lambda_a}{\varepsilon - \lambda}\left[1 - e^{-(\varepsilon-\lambda)t}\right] + \left(\frac{^{40}\mathrm{Ar}}{^{40}\mathrm{K}}\right)_0 e^{-(\varepsilon-\lambda)t} \tag{15}$$

where the initially present radiogenic ^{40}Ar is represented by the term $(^{40}\mathrm{Ar}/^{40}\mathrm{K})_0$. The initial ratio may be either greater or less than the measured one depending on the production and escape rates. A mineral fraction may initially contain ^{40}Ar trapped during formation, or resulting from admixture of older detrital particles. Although such cases are, in principle, represented by equation 15 where production and loss occur simultaneously, it is not always possible to determine the initial ^{40}Ar concentration in a size fraction, leading us to consider the finest fraction as newly formed and initially free of radiogenic ^{40}Ar. With no initial radiogenic ^{40}Ar and no escape from the system ($\varepsilon = 0$), equation 15 becomes identical to the closed-system case as given in equation 10. With no initial ^{40}Ar, equation 15 can be written as:

$$\frac{^{40}\mathrm{Ar}}{^{40}\mathrm{K}} = \frac{\lambda_a}{\varepsilon - \lambda}[1 - e^{-(\varepsilon-\lambda)t}] \tag{16}$$

An ^{40}Ar escape rate greater than the decay rate of ^{40}K corresponds to the condition of $\varepsilon > \lambda$, making it theoretically possible to attain a steady state as t increases indefinitely. Parenthetically, it may be noted that in a closed system, as represented by equations 10 and 11, no steady state can be attained except in a mathematical sense of no production of ^{40}Ar after an infinitely long time. A steady-state value of the ^{40}Ar/^{40}K ratio in equation 16 is:

$$\frac{^{40}\mathrm{Ar}}{^{40}\mathrm{K}} = \frac{\lambda_a}{\varepsilon - \lambda} \tag{17}$$

The physical significance of a constant ^{40}Ar/^{40}K ratio in equation 17 is that both the ^{40}Ar and ^{40}K concentrations decrease with time in the sediment and ^{40}Ar is lost at a rate greater than the decay rate of its parent ^{40}K, of which only a fraction produces ^{40}Ar. The ^{40}Ar escape-rate parameter ε, in equations 12 and 16, is constrained at the lower bound by $\varepsilon = \lambda$ and at the upper bound by the steady-state ^{40}Ar/^{40}K ratio. If ε is close to λ, so that the difference $(\varepsilon - \lambda) \approx 0$, then the ^{40}Ar/^{40}K ratio becomes a linear function of time in equation 16:

$$\frac{^{40}\mathrm{Ar}}{^{40}\mathrm{K}} = \lambda_a t \tag{18}$$

As the difference $(\varepsilon - \lambda)$ tends to 0, the numerator and denominator in equation 16 tend to a ratio of 0/0; the result in equation 18 is obtained by differentiating the numerator and denominator in equation 16 with respect to $(\varepsilon - \lambda)$ and taking the limit of $(\varepsilon - \lambda) \to 0$. In Figure 5 are shown curves for an increase in the ^{40}Ar/^{40}K ratio in a closed system and in an open system

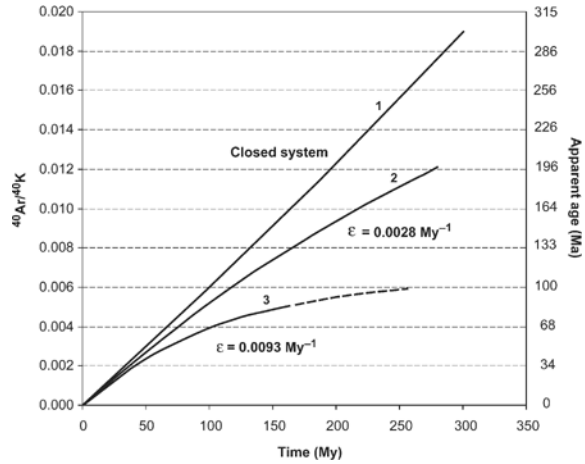

Figure 5. $^{40}Ar/^{40}K$ atomic ratios as a function of time in: (1) a closed system, equation 10; (2) production and escape model, equation 16, ^{40}Ar escape-rate parameter, ε, is the mean value of the two Permian estimates (Table 3); (3) escape-rate parameter, ε, is the mean of the two higher values estimated for the Mesozoic section of the North Sea (Table 3). Note that a higher value of escape rate, ε, makes the apparent age younger and the system approach a steady state faster.

with production and escape as a function of time. For a closed system, the curves show true ages, whereas for an open system, one escape rate parameter is the mean of the values for the Permian ($\varepsilon = 2.8 \times 10^{-9}$ y^{-1}) and the other is for the Mesozoic authigenic illite and I-S fractions ($\varepsilon = 9.3 \times 10^{-9}$ y^{-1}).

ESTIMATION OF ^{40}Ar ESCAPE RATE PARAMETER, ε

As the small-size authigenic particles are less likely to contain inherited ^{40}Ar, we shall first discuss their diagenesis in terms of equation 16 where newly formed particles lose ^{40}Ar after formation. In this model, the duration of the ^{40}Ar production and escape takes place over a period of time not greater than the stratigraphic age and not less than the K-Ar apparent age. Relationship 16 has two unknowns: the time since the particles formed, t, and the rate of ^{40}Ar escape, ε, resulting in the observed $^{40}Ar/^{40}K$ ratios. Thus, in the case of a non-steady state, equation 16 can give only values of the escape-rate parameter, ε, that depend on a reasonable choice of t.

To obtain estimates of the escape rate for the Permian section (Table 3), we assume that the process started at 275 Ma, the midpoint of the stratigraphic time interval. Then it follows from equation 16, that the <2 μm fraction of K-Ar apparent age 184 Ma is characterized by an escape rate $\varepsilon = 3.3 \times 10^{-9}$ y^{-1}. For the 204 Ma-old fraction, the escape rate is $\varepsilon = 2.3 \times 10^{-9}$ y^{-1}. If the starting time is considered to be the same, a faster escape rate is needed to attain a smaller $^{40}Ar/^{40}K$ ratio corresponding to a younger K-Ar apparent age of 184 Ma. For the neoformed I-S in the North Sea section of K-Ar apparent age of 78 Ma, a choice of the starting time between 100 and 160 Ma gives an ^{40}Ar escape rate, ε, ranging from 5.3×10^{-9} to 10.6×10^{-9} y^{-1}. For a given K-Ar apparent age, the relationship between t and ε stems from equation 16, where ε appears in both the exponential term and the denominator of the first term. In the production and escape model, a lower limit of ε is $\varepsilon = \lambda = 0.5543 \times 10^{-9}$ y^{-1}. At this value of ε, equation 18 gives approximately the K-Ar apparent ages of the authigenic minerals (Table 3). In the Tertiary Gulf Coast sediments (Table 3), it is not certain which part of the <0.1 μm fraction was newly formed by addition of K, insofar as it yields an age of 35 Ma comparable to the stratigraphic age (Aronson and Hower, 1976). Strictly speaking, this uncertainty makes questionable an application of the ^{40}Ar production and escape model to the finest fraction of this example. If the formation of the authigenic phase started between 25 and 32 Ma ago, the ^{40}Ar escape-rate parameter from equation 16 is $\varepsilon = 25 \times 10^{-9}$ to 38×10^{-9} y^{-1}.

It is important to state here that the nearly constant $^{40}Ar/^{40}K$ ratios in the Permian, Mesozoic and Tertiary sections (Figure 4) cannot result from a steady state. If the $^{40}Ar/^{40}K$ ratios from 0.0126 to 0.00462 (Table 3) were interpreted as steady-state ratios, the escape-rate parameter, ε, of equation 17, would be 5.2×10^{-9} to 13×10^{-9} y^{-1} instead of 2.3×10^{-9} and 5.2×10^{-9}. For a steady state to be nearly attained, the exponential term on the right-hand side of equation 16 should be less than unity, at $e^{-3} \approx 0.05$. With a steady-state ε value of ~0.013 per Ma for the Mesozoic North Sea section, the condition for the power exponent in equation 16 to be $(\varepsilon - \lambda)t = 3$ would be attained after 245 Ma, which is somewhat greater than the stratigraphic age of the section. For the Permian section, the time to steady state, as measured by the value of t in $(\varepsilon - \lambda)\, t = 3$ would be reached after 645 to 580 Ma, which is far greater than the stratigraphic age.

For the Neogene sequence of Kalimantan (Table 3), the K-Ar apparent age of the heterogeneous <0.4 μm fraction is greater than the depositional age. As it contains inherited minerals with $^{40}Ar/^{40}K$ ratios of the coarser fraction, the post-depositional ^{40}Ar loss amounts to 38±2%. However, if the recently identified smaller fundamental particles of K-Ar apparent age equal to 14 Ma are taken in terms of ^{40}Ar production with escape starting 17 Ma ago, then the ^{40}Ar escape-rate parameter is $\varepsilon = 7.2 \times 10^{-9}$ y^{-1}.

CONCLUSIONS

Preferential loss of ^{40}Ar from small particles of submicrometer size, relative to the bigger particles occurring in the same sedimentary units, has been described by many investigators since the 1960s. We quantify some published K-Ar results in terms of fractional losses

of ^{40}Ar from the small-size fractions (<0.2 to <0.5 μm particle diameter) relative to the larger (up to 20–40 μm). As a whole, the smallest fractions of the Paleozoic samples are characterized by the smallest relative losses of 15–26% relative to the larger 10–20 to 2–6 μm fractions. The <0.4 μm fractions of the Mesozoic section show a somewhat greater loss of 33–39%, followed by the Tertiary section where the estimated loss is ~50% for fractions in a size range from <0.5 to 2–10 μm.

Estimation of ^{40}Ar loss based on a model of diffusional loss from spherical particles gives higher values of ^{40}Ar fractions lost from the smallest particles but it preserves the trend of relatively smaller losses of 38±10% in Paleozoic sediments, greater losses of 48±9%, in the Lower Mesozoic, and the highest losses of 65±8% in the Tertiary and Neogene. The main uncertainties behind the discrepancies between the estimates are, at least in part, due to the nature of the data: (1) uneven size classes reported in the different sets of analyses; (2) heterogeneity of the smaller fractions that may contain detrital contaminants of older age together with varied proportions of different clays; (3) aggregation of smaller particles into bigger particles or, conversely, fracturing of bigger particles; and (4) a general lack of knowledge of the pre-diagenetic state of the sediment particles. Other uncertainties are attributable to simplifications and approximations in the mathematical models that were introduced in dealing with the limitations of the available data. The high values of ^{40}Ar fractions lost from the small fractions of the Neogene in Kalimantan and of the Miocene-Oligocene in the Gulf Coast confirm that reducing the K-Ar apparent age and the $^{40}Ar/^{40}K$ ratios is due to addition of ^{40}K on top of the loss of ^{40}Ar, to and from different mineral constituents of the fine fraction.

Sedimentary sections from a few hundreds to >1500 m thick, where authigenic K-bearing clays (mixed-layer illite-smectite and illite) show no systematic trends in K-Ar apparent ages and $^{40}Ar/^{40}K$ ratios, varying about a mean value, occur in the Permian of North Germany, the Mesozoic of the North Sea, and the Tertiary of the Gulf Coast. The K-Ar apparent ages of the authigenic minerals in the small fractions are younger than the stratigraphic age, so that the $^{40}Ar/^{40}K$ ratios in these sections are interpreted as due to a balance between ^{40}Ar production and loss by a first-order escape flux. Computed values of the escape-rate parameter, ε, range from 0.2×10^{-8} to 4×10^{-8} y^{-1} depending on their K-Ar apparent ages and the length of time since the start of the formation of the authigenic fractions. In a system with ^{40}Ar production and escape, a steady state of the $^{40}Ar/^{40}K$ ratio is, in principle, attainable, but the length of time needed to attain it is too great for the stratigraphic ages of the studied sections.

In summary, the proposed model for radiogenic ^{40}Ar loss in fine-clay sized sediments is at a preliminary stage as more controlling factors still need to be included in the calculation, especially the aspects of combined accumulation and loss of radiogenic ^{40}Ar in the smallest authigenic-enriched size fractions. However, two aspects might be raised at this juncture: (1) on the basis of the varied types of rocks considered, in basins with varied evolutionary pathways, the model results can certainly be used for other sequences deposited in similar conditions; and (2) the consistency of the estimates underline the reliability of the K-Ar analytical data made previously on clay material, on the basis of a routine elaborated and presented elsewhere.

ACKNOWLEDGMENTS

This work was supported by the Agence Nationale pour la Gestion des Déchets Radioactifs (ANDRA, Chatenay-Malabry, France), U.S. National Science Foundation Grants OAR-0002889 and EAR-02-23509, and the A. L. Howland Fund of the Department of Geological Sciences, Northwestern University. We are grateful to these organizations for their support, to A. Clement (CGS, Strasbourg) for his dedicated and imaginative resolution of the software and computer-network issues, and to A. Bouzeghaia (CGS, Strasbourg) for graphical work. We also thank Associate Editor W. Huff (University of Cincinnatti) and B. Lang (Geological Survey of Israel) for their very constructive comments, as well as C. M. Hall (University of Michigan) for an earlier review. This is publication No. 2004.304 of EOST, Université Louis Pasteur, Strasbourg, France.

REFERENCES

Aronson, J.L. and Hower, J. (1976) Mechanism of burial metamorphism of argillaceous sediments: 2. Radiogenic argon evidence. *Geological Society of America Bulletin*, **87**, 738–744.

Aronson, J.L. and Lee, M.C. (1986) K/Ar systematics of bentonite and shale in contact metamorphic zone, Cerrilos, New Mexico. *Clays and Clay Minerals*, **34**, 483–487.

Carslaw, H.S. and Jaeger, J.C. (1959) *Conduction of Heat in Solids*, 2nd edition. Oxford University Press, Oxford, x + 520 pp.

Clauer, N. and Chaudhuri, S. (1995) *Clays in Crustal Environments – Isotope Dating and Tracing*. Springer-Verlag, New York, 359 pp.

Clauer, N., O'Neil, J.R. and Furlan, S. (1995) Clay minerals as records of temperature conditions and duration of thermal anomalies in the Paris Basin, France. *Clay Minerals*, **30**, 1–13.

Clauer, N., O'Neil, J.R. and Bonnot-Courtois, C. (1982) The effect of natural weathering on the chemical and isotopic compositions of biotites. *Geochimica et Cosmochimica Acta*, **46**, 1755–1762.

Clauer, N., Rinckenbach, T., Weber, F., Sommer, F., Chaudhuri, S. and O'Neil, J.R. (1999) Diagenetic evolution of clay minerals in oil-bearing Neogene sandstones and associated shales, Mahakam Delta Basin, Kalimantan, Indonesia. *American Association of Petroleum Geologists Bulletin*, **83**, 62–87.

Clauer, N., Zwingmann, H. and Gorokhov, I.M. (2003) Postdepositional evolution of platform claystones based on a simulation of thermally induced diffusion of radiogenic

^{40}Ar from diagenetic illite. *Jounal of. Sedimentary Research*, **73**, 58–63.

Clauer, N., Rousset, D. and Środoń, J. (2004) Modeled shale and sandstone burial diagenesis based on the K-Ar systematics of illite-type fundamental particles. *Clays and Clay Minerals*, **52**, 576–588.

Crank, J. (1967) *Mathematics of Diffusion*, 2nd edition. Oxford University Press, Oxford, UK, viii + 424 pp.

Dalrymple, G.B. and Lanphere, M.A. (1969) *Potassium-Argon Dating*. Freeman, San Francisco, 258 pp.

Dodson, M.H. (1973) Closure temperature in cooling geochronological and petrological systems. *Contributions to Mineralogy and Petrology*, **40**, 259–274.

Dong, H., Hall, C.M., Peacor, D.R. and Halliday, A.N. (1995) Mechanisms of argon retention in clays revealed by laser ^{40}Ar-^{39}Ar dating. *Science*, **267**, 355–359.

Dong, H., Hall, C.M., Halliday, A.N. and Peacor, D.R. (1997) ^{40}Ar–^{39}Ar dating of Late-Caledonian (Acadian) metamorphism and cooling of K-bentonites and slates from the Welsh Basin, U.K. *Earth and Planetary Science Letters*, **150**, 337–351.

Dong, H., Hall, C.M., Peacor, D.R. Halliday, A.N. and Pevear, D.R. (2000) Thermal ^{40}Ar/^{39}Ar separation of diagenetic from detrital illitic clays in Gulf Coast shales. *Earth and Planetary Science Letters*, **175**, 309–325.

Eberl, D.D. (1993) Three zones for illite formation during burial diagenesis and metamorphism. *Clays and Clay Minerals*, **41**, 26–37.

Faure, G. (1986) *Principles of Isotope Geology*, 2nd edition. Wiley, New York, xv + 589 pp.

Folger, H.W., Snee, L.W., Mehnert, H.H. and Hofstra, A.H. (1995) Significance of K-Ar and 40Ar/39Ar dates from mica in Carlin-type gold deposits: Evidence from the Jerritt Canyon District, Nevada. Pp. 41–60 in: *Geology and Ore Deposits of the Merica Cordillera* (A. R. Coyner and P. L. Fahey, editors). Geological Society of Nevada Symposium Proceedings, Reno/Sparks, Nevada, USA.

Folger, H.W., Hofstra, A.H., Eberl, D.D. and Snee, L.W. (1998) Importance of clay characterization to interpretation of ^{40}Ar/^{39}Ar dates of illite from Carlin-type gold deposits: insights from Jerritt Canyon, Nevada: U.S. Geological Survey Open File Report, **98-338**, pp. 193–201.

Freer, R. (1981) Diffusion in silicate minerals and glasses: a data digest and guide to literature. *Contributions to Mineralogy and Petrology*, **76**, 440–454.

Furlan, S. (1994) Transferts de matière au cours de la diagenèse d'enfouissement dans le bassin du delta de la Mahakam (Indonésie). Un nouveau concept pour le mécanisme de l'utilsation. Thèse de Doctorat, Université Louis Pasteur, Institut de Géologie, Strasbourg, France, 224 pp.

Furlan, S., Clauer, N., Chaudhuri, S. and Sommer, F. (1996) K transfer during burial diagenesis in the Mahakam Delta Basin (Kalimantan, Indonesia). *Clays and Clay Minerals*, **44**, 157–169.

Glasmann, J.R., Larter, S., Briedis, N.A. and Lundegard, P.D. (1989) Shale diagenesis in the Bergen High Area, North Sea. *Clays and Clay Minerals*, **37**, 97–112.

Hall, C.M., Higueras, P., Kesler, S.E., Lunar, R., Dong, H. and Halliday, A.N. (1997) Dating of alteration episodes related to mercury mineralization in the Almadén district, Spain. *Earth and Planetary Science Letters*, **148**, 287–298.

Hamilton, P.J., Kelley, S. and Fallick, A.E. (1989) K-Ar dating of illite in hydrocarbon reservoirs. *Clay Minerals*, **24**, 213–215.

Harland, W.B., Armstrong, R.L., Cox, A.V., Craig, L.E., Smith, A.G. and Smith, D.G. (1990) *A Geologic Time Scale 1989*. Cambridge University Press, Cambridge, UK, 263 pp.

Hower, J., Eslinger, E.V., Hower, M.E. and Perry, E.A. Jr. (1976) Mechanism of burial metamorphism of argillaceous sediment: 1. Mineralogical and chemical evidence. *Geological Society of America Bulletin*, **87**, 725–737.

Huon, S., Cornée, J.J., Piqué, A., Rais, N., Clauer, N., Liewig, N. and Zayane, R. (1993) Mise en évidence au Maroc d'événements thermiques d'âge triasico-liasique liés à l'ouverture de l'Atlantique. *Bulletin de la Société géologique de France*, **164**, 165–176.

Langley, K.M. (1978) Dating sediments by the K-Ar method. *Nature*, **276**, 56–57.

Lerman, A. (1979) *Geochemical Processes – Water and Sediment Environments*. Wiley, New York, viii + 481 pp.

Liewig, N. and Clauer, N. (2000) K-Ar dating of varied microtextural illite in Permian gas reservoirs, northern Germany. *Clay Minerals*, **35**, 275–285.

Liewig, N., Clauer, N. and Sommer, F. (1987) Rb-Sr and K-Ar dating of clay diagenesis in Jurassic sandstone reservoirs. *American Association of Petroleum Geologists Bulletin*, **71**, 1467–1474.

Lovera, O.M. (1992) Computer programs to model ^{40}Ar/^{39}Ar diffusion data from multidomain samples. *Computers & Geoscience*, **18**, 789–813.

McDougall, I. and Harrison, T.M. (1999) *Geochronology and Thermochronology by the ^{40}Ar/^{39}Ar Method*, 2nd edition. Oxford University Press, New York, xii + 269 pp.

Mitchell, J.G. and Taka, A.S. (1984) Potassium and argon loss patterns in weathered micas: implications for detrital mineral studies with particular reference to the Triassic paleogeography of the British Isles. *Sedimentary Geology*, **39**, 27–52.

Mossmann, J.R., Clauer, N. and Liewig, N. (1992) Dating thermal anomalies in sedimentary basins: the diagenetic history of clay minerals in the Triassic sandstones of the Paris Basin (France). *Clay Minerals*, **27**, 211–226.

Perry, E.A. Jr. (1974) Diagenesis and the K-Ar dating of shales and clay minerals. *Geological Society of America Bulletin*, **85**, 827–830.

Priyomarsono, S. (1985) *Contribution à l'étude géologique du Sud-Est de Bornéo (Indonésie)*. Université de Savoie, Département des Sciences de la Terre, France, **5**, 172 pp.

Reuter, A. (1987) Implications of K-Ar ages of whole-rock and grain-size fractions of metapelites and intercalated metatuffs within an anchizonal terrane. *Contributions to Mineralogy and Petrology*, **97**, 105–115.

Schaltegger, U., Zwingmann, H., Clauer, N., Larqué, P. and Stille, P. (1995) K-Ar dating of a Mesozoic hydrothermal activity in Carboniferous to Triassic clay minerals of northern Switzerland. *Schweizerische Mineralogische und Petrographische Mitteilungen*, **75**, 163–176.

Shackleton, N.J., Hall, M.A., Raffi, I., Tauxe, L. and Zachos, J. (2000) Astronomical calibration age for the Oligocene-Miocene Boundary. *Geology*, **28**, 447–450.

Steiger, R.H. and Jäger, E. (1977) Subcommission on Geochronology: Convention on the use of decay constants in geo- and cosmochronology. *Earth and Planetary Science Letters*, **36**, 359–362.

Turner, G. (1968) The distribution of potassium and argon in chondrites. Pp. 387–398 in: *Origin and Distribution of the Elements* (L.H. Ahrens, editor). Pergamon Press, Oxford, UK.

Weaver, C.E. and Broekstra, B.R. (1984) Illite-mica. Pp. 99–139 in: *Shale-Slate Metamorphism in Southern Appalachians* (C.E. Weaver, editor). Elsevier, Amsterdam.

Wijbrans, J.R. and McDougall, I. (1986) ^{40}Ar/^{39}Ar dating of white micas from an Alpine high-pressure metamorphic belt of Naxos (Greece): the resetting of the argon isotopic system. *Contributions to Mineralogy and Petrology*, **93**, 187–194.

Wilson, G.S., Lavelle, M., McIntosh, W.C., Roberts, A.P., Harwood, D.M., Watkins, D.K., Villa, G., Bohaty, S.M.,

Fielding, C.R., Florindo, F., Sagnotti, L., Naish, T.R. and Scherer, R.P. (2002) Integrated chronostratigraphic calibration of the Oligocene-Miiocene boundary at 24.0±0.1 Ma from the CRP-2A drill core, Ross Sea, Antarctica. *Geology*, **30**, 1043–1046.

Zwingmann, H. (1995) Study of the conditions of gas emplacement in sandstone reservoirs (Rotliegende of Germany). Mineralogical, morphological, geochemical and isotopical aspects. Doctoral Thesis, Université Louis Pasteur, Institut de Géologie, Strasbourg, France, 210 pp.

Zwingmann, H., Clauer, N. and Gaupp, R. (1999) Structure-related geochemical (REE) and isotopic (K-Ar, Rb-Sr, $\delta^{18}O$) characteristics of clay minerals from Rotliegend sandstone reservoirs (Permian, northern Germany). *Geochimica et Cosmochimica Acta*, **63**, 2805–2823.

(*Received 6 February 2004; revised 7 January 2005; Ms. 880; A.E. Warren D. Huff*)